Available online at www.sciencedirect.com
ScienceDirect
Journal of Power Sources 161 (2006) 707–722
JOURNAL OF POWER SOURCES
www.elsevier.com/locate/jpowsour

Dynamic modeling, design and simulation of a wind/fuel cell/ultra-capacitor-based hybrid power generation system

O.C. Onar, M. Uzunoglu, M.S. Alam *

Department of Electrical and Computer Engineering, University of South Alabama, Mobile, AL 36688, USA

Received 24 February 2006; received in revised form 17 March 2006; accepted 28 March 2006
Available online 18 May 2006

Abstract

Recent research and development of alternative energy sources have shown excellent potential as a form of contribution to conventional power generation systems. In order to meet sustained load demands during varying natural conditions, different energy sources and converters need to be integrated with each other for extended usage of alternative energy. The paper focuses on the combination of wind, fuel cell (FC) and ultra-capacitor (UC) systems for sustained power generation. As the wind turbine output power varies with the wind speed: an FC system with a UC bank can be integrated with the wind turbine to ensure that the system performs under all conditions. We propose herein a dynamic model, design and simulation of a wind/FC/UC hybrid power generation system with power flow controllers. In the proposed system, when the wind speed is sufficient, the wind turbine can meet the load demand while feeding the electrolyzer. If the available power from the wind turbine cannot satisfy the load demand, the FC system can meet the excess power demand, while the UC can meet the load demand above the maximum power available from the FC system for short durations. Furthermore, this system can tolerate the rapid changes in wind speed and suppress the effects of these fluctuations on the equipment side voltage in a novel topology.

Keywords: Dynamic model; Wind power; Fuel cell; Ultra-capacitor; Renewable energy and hybrid power generation

1. Introduction

The dependence of economy on depleting fossil fuels and the adverse environmental effects of conventional power generation systems created renewed interest in renewable energy sources toward building a sustainable energy economy in the next decade. Wind energy is the world's fastest growing energy source, expanding globally at a rate of 25–35% annually over the last decade [1]. The main disadvantage of wind turbines is that naturally variable wind speed causes voltage and power fluctuation problems at the load side. This problem can be solved by using appropriate power converters and control strategies. Another significant problem is to store the energy generated by wind turbines for future use when no wind is available but the user demand exists [2]. As a solution for this energy storage problem, wind energy after appropriate conversion can be stored in the form of hydrogen which will be converted to electrical energy via fuel cells (FCs). This type of energy storage provides significant advantages when compared to conventional batteries in terms of energy density and long-term storage [2,3]. By using an electrolyzer, hydrogen conversion allows both storage and transportation of large amounts of power at much higher energy densities [3]. Thus, hydrogen generation can lead a pathway for wind-based energy generation to contribute directly to reducing the dependence on imported fossil fuel [4,5]. According to Ref. [6,7], wind electrolysis is an attractive candidate for economically viable renewable-hydrogen production system. Furthermore, coupling wind turbines with electrolyzers has the potential to provide low-cost, environmentally friendly distributed generation of hydrogen in addition to electricity [4]. Thus, the stored hydrogen energy can be used by FC power plants during the low wind speed conditions.

FC power plants use oxygen and hydrogen to convert chemical energy into electrical energy. Among the various types of FC systems, proton exchange membrane (PEM) FC power plants have been found to be especially suitable for hybrid energy systems with higher power density and lower operating temperature. However, assisting an FC power plant with a parallel

* Corresponding author. Tel.: +1 251 460 6117; fax: +1 251 460 6028.
E-mail address: malam@usouthal.edu (M.S. Alam).

0378-7753/$ – see front matter © 2006 Elsevier B.V. All rights reserved.
doi:10.1016/j.jpowsour.2006.03.055

ultra-capacitor (UC) bank makes economic sense when satisfying the peak power demands or transient events. Ultra-capacitors are electrical energy storage devices with extremely high capacitance values (a few Farads to several thousand Farads per cell) offering high energy densities when compared to conventional capacitors [8]. Without the UC bank, the FC system must supply all power demand thus increasing the size and cost of the FC power plant.

Some studies have been reported in the literature to model hybrid renewable energy systems, FC power plants, and other relevant areas. Among them, Khan et al. [2,9] presented the model of a small wind-fuel cell hybrid energy system and analyzed life cycle of a wind-fuel cell integrated system. Delfino and Fornari [10] investigated a grid integrated fuel cell-wind turbine system. In Ref. [3], power conditioning for a wind-hydrogen energy system has been reported. Bechrakis et al. [11] investigated simulation and operational assessment for a small autonomous wind-hydrogen energy system. Barbir [12] proposed a system for the production of hydrogen from renewable energy sources using PEM electrolysis. In Ref. [13], a dynamic model of a PEM electrolyzer and a hydrogen storage model is introduced. Mathematical modeling and simulation of dynamic systems are important in order to develop the best hybrid system.

In this paper, a detailed dynamic model, design and simulation of a wind/FC/UC-based hybrid power generation system is developed using a novel topology to complement each other and to alleviate the effects of wind speed variations. The dynamic PEMFC/UC hybrid power system model reported in Ref. [14] is modified for this study, and integrated with the wind turbine, generator, electrolyzer and storage models. Modeling and simulations are performed using MATLAB, Simulink and SimPowerSystems [15–17] software packages to verify the effectiveness of the proposed system.

2. System description

In this section, the dynamic simulation model is described for the wind/FC/UC hybrid generation system. The developed system consists of a wind turbine, an induction generator with power factor correction capacitor bank, an ac/dc thyristor controlled double-bridge rectifier with PI controlled firing angle, an FC/UC system with a boost type dc/dc converter with PI controlled duty cycle, two dc/ac IGBT inverters with 5 kHz carrier signal, and a two-winding coupling transformer located at the load side. The block diagram of the integrated overall system is shown in Fig. 1.

2.1. Design and dynamic model of a wind turbine

In the literature, several studies have been reported regarding wind turbines and wind power driven generators [2,3,10,18]. The model proposed in this paper is based on the wind speed versus wind turbine output power characteristics. The parameters used in the mathematical modeling of the wind turbine are as follows:

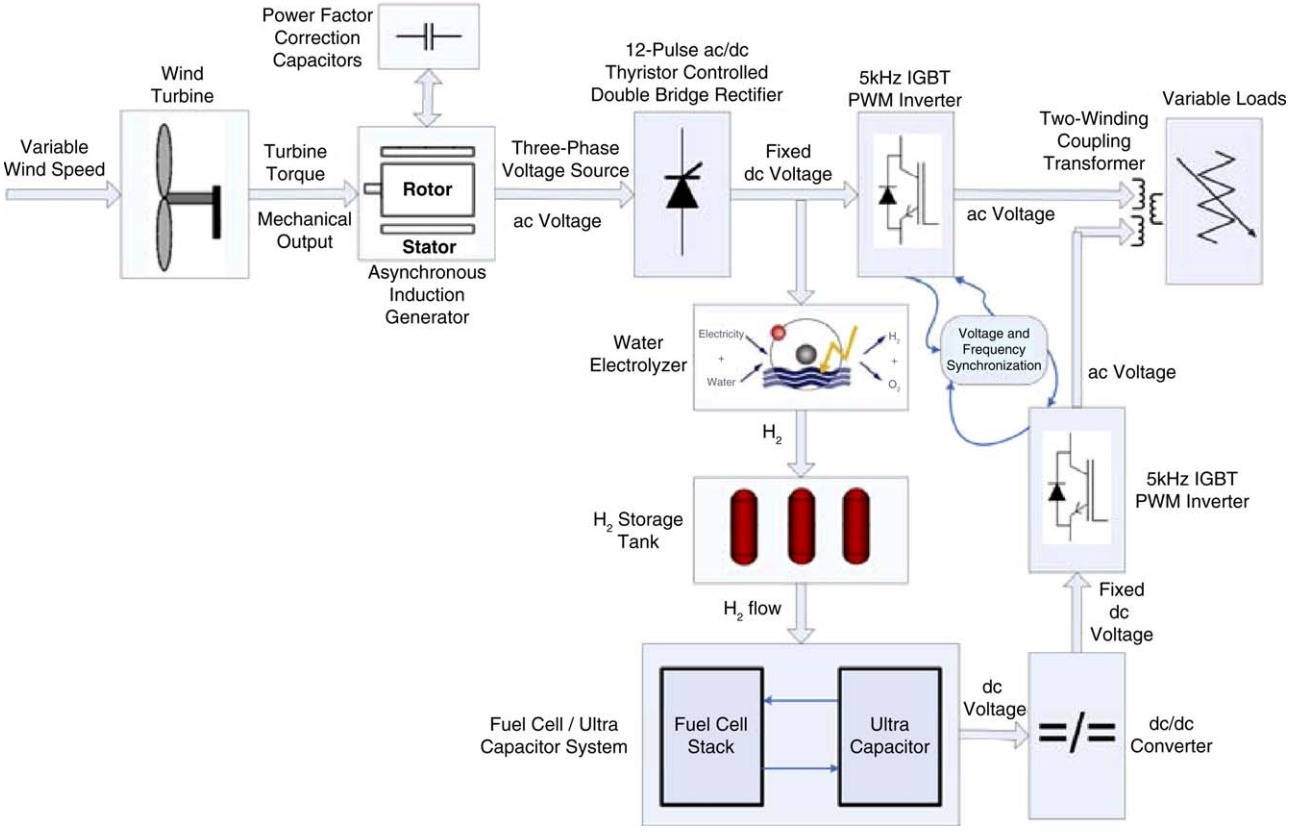

Fig. 1. Block diagram of the proposed system.

A turbine swept area [m^2]
c_p performance coefficient of the turbine
c_{p_pu} per unit (p.u.) value of the performance coefficient c_p
k_p power gain for $c_{p\_pu} = 1$ and $\upsilon_{wind\_pu} = 1$ p.u., $k_p \leq 1$
P_m mechanical output power of the turbine [W]
P_{m_pu} power in p.u. of nominal power for particular values of ρ and A
β blade pitch angle [°]
λ tip speed ratio of the rotor blade tip speed to wind speed
ρ air density [kg $(m^3)^{-1}$]
υ_{wind} wind speed [m s^{-1}]
υ_{wind_pu} p.u. value of the base wind speed. The based wind speed is the mean value of the expected wind speed in (m s^{-1}).

The output power of the wind turbine is given by [17,19,20]

$$P_m = c_p(\lambda,\ \beta)\frac{\rho A}{2}\upsilon_{wind}^3. \quad (1)$$

Eq. (1), can be normalized and simplified for specific values of ρ and A. The new equation in per unit (p.u.) system can be expressed as

$$P_{m\_pu} = k_p c_{p\_pu}\upsilon_{wind\_pu}^3. \quad (2)$$

The modified Simulink model of the turbine is illustrated in Fig. 2 [17,19,20]. In this model, whereas the inputs are the generator speed and wind speed, the output is mechanical torque applied to the induction generator shaft.

2.2. Design and dynamic model of an asynchronous induction generator

In this study, the built-in SimPowerSystems block model of an asynchronous induction machine is used as a power generator driven by the wind turbine [17]. In this model, the electrical and mechanical parts of the machine are built following the procedure described in Ref. [21].

The asynchronous induction generator model parameters used in this model are as follows:

E_s stator induced voltage per phase
F combined rotor and load viscous friction coefficient
f_n nominal frequency
H combined rotor and load inertia constant
I_s stator current
n_s synchronous rotations per minute
p number of pole pairs
P_e electrical power output
P_m mechanical input power
R'_s combined rotor and stator resistance and inductance
L'_s referred to stator
S_n apparent power output
T_e electromagnetic torque
T_m shaft mechanical torque
V_s stator terminal voltage per phase
δ power angle
θ_m rotor angular position
ω_m angular velocity of the rotor

In an asynchronous machine, the synchronous speed and the angular velocity of the rotor can be expressed as

$$n_s = \frac{60}{p}f_n, \quad (3)$$

$$\omega_m = \frac{2\pi}{60}n_s. \quad (4)$$

The mechanical torque which drives the rotor shaft yields the mechanical input power as

$$P_m = T_m\omega_m. \quad (5)$$

Then the derivative of angular velocity and the angular position of the rotor becomes

$$\frac{d}{dt}\omega_m = \frac{1}{2H}(T_e - F\omega_m - T_m), \quad (6)$$

and

$$\frac{d}{dt}\theta_m = \omega_m. \quad (7)$$

The relationship between the induced and terminal voltage of the stator windings is given by

$$V_s = E_s - (R'_s + j2\pi f L'_s)I_s. \quad (8)$$

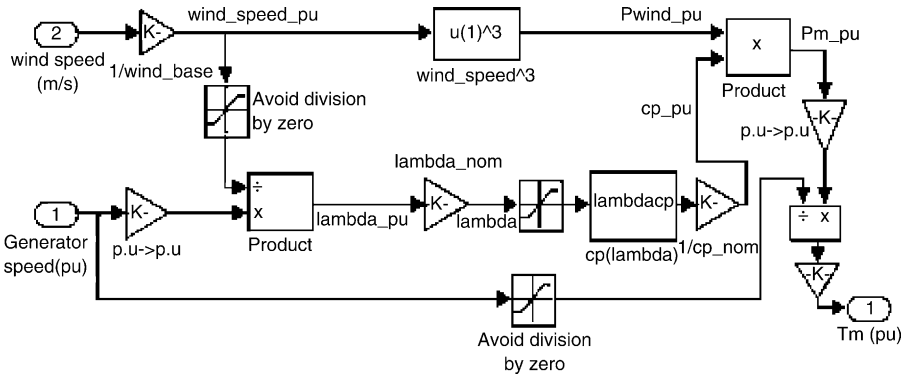

Fig. 2. Simulink model of the wind turbine.

The apparent power output of the induction generator can be defined as

$$S_n = 3V_s I_s^*. \tag{9}$$

The electrical active power output of the induction machine is given by

$$P_e = 3\frac{E_s V_s}{\sqrt{R_s'^2 + (2\pi f L_s')^2}} \sin\delta. \tag{10}$$

In this study, the rotor windings of the generator are short circuited (squirrel cage induction machine) and the rotor shaft is driven by the wind turbine which produces the mechanical torque according to the wind and generator speed values. The loads are connected to the electrical power output of the generator, i.e., stator windings.

2.3. Design and dynamic modeling of a PEMFC

The PEMFC model described in Ref. [14] and Ref. [22] is modified in MATLAB and Simulink for this study. This model is built using the relationship between output voltage and partial pressure of hydrogen, oxygen and water. Fig. 3 shows the detailed model of the PEMFC, which is then embedded into the SimPowerSystems of MATLAB as a controlled voltage source and integrated into the overall system. The FC system model parameters used in this model are as follows:

B, C	constants to simulate the activation over voltage in PEMFC system [A^{-1}] and [V]
E	Nernst instantaneous voltage [V]
E_0	standard no load voltage [V]
F	Faraday's constant [C kmol^{-1}]
I_{FC}	FC system current [A]
K_{an}	anode valve constant [K mol kg (atm s)$^{-1}$)]
K_{H_2}	hydrogen valve molar constant [kmol (atm s)$^{-1}$]
K_{H_2O}	water valve molar constant [kmol (atm s)$^{-1}$]
K_{O_2}	oxygen valve molar constant [kmol (atm s)$^{-1}$]
K_r	modeling constant [kmol (s A)$^{-1}$]
M_{H_2}	molar mass of hydrogen [kg kmol^{-1}]
N_0	number of series fuel cells in the stack
P_{H_2}	hydrogen partial pressure [atm]
P_{H_2O}	water partial pressure [atm]
P_{O_2}	oxygen partial pressure [atm]
q_{O_2}	input molar flow of hydrogen [kmol s^{-1}]
$q_{H_2}^{in}$	hydrogen input flow [kmol s^{-1}]
$q_{H_2}^{out}$	hydrogen output flow [kmol s^{-1}]
$q_{H_2}^{r}$	hydrogen flow that reacts [kmol s^{-1}]
$q_{H_2}^{req}$	amount of hydrogen flow required to meet the load change (kmol s^{-1})
R	universal gas constant [(1 atm) (kmol K)$^{-1}$]
R^{int}	FC internal resistance [Ω]
R_{H-O}	the hydrogen–oxygen flow ratio
T	absolute temperature [K]
U	utilization rate
V_{an}	volume of the anode [m^3]
V_{cell}	dc output voltage of FC system [V]
τ_{H_2}	hydrogen time constant [s]
τ_{O_2}	oxygen time constant [s]
τ_{H_2O}	water time constant [s]
η_{act}	activation over voltage [V]
η_{ohmic}	Ohmic over voltage [V]

In MATLAB, "log 10" and "log" are used as logarithmic commands within the Simulink blocks as shown in Fig. 3. We used base-10 logarithm in the Nernst equation and base-e logarithm in the activation voltage equation. Also, in the Simulink model of the FC system, the input variables of the function blocks must be denoted with lowercase 'u' as shown in Fcn1, Fcn2 and Fcn3 blocks.

The FC system consumes hydrogen according to the power demand, where hydrogen is obtained from the storage tank. To control the hydrogen flow rate according to the FC power output, a feedback control strategy is utilized by taking output FC current back to the input.

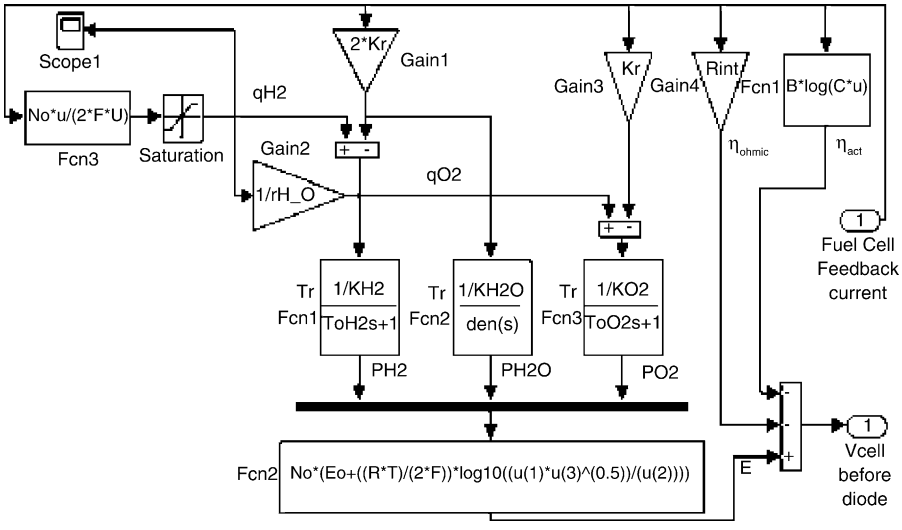

Fig. 3. Dynamic model of the FC system.

2.4. Design and dynamic modeling of ultra-capacitor bank

The parameters used in the mathematical modeling of the UC bank are as follows:

C	capacitance [F]
$C_{\text{UC-total}}$	the total UC system capacitance [F]
EPR	equivalent parallel resistance [Ω]
ESR, R	equivalent series internal resistance[Ω]
E_{UC}	the amount of energy released or captured by the UC bank [W s]
n_{s}	the number of capacitors connected in series
n_{p}	the number of series strings in parallel
$R_{\text{UC-total}}$	the total UC system resistance [Ω]
V_{i}	the initial voltage before discharging starts [V]
V_{f}	the final voltage after discharging ends [V]

Fig. 4 shows the classical equivalent circuit of the UC unit. The model consists of a capacitance (C), an equivalent series resistance (ESR, R) representing the charging and discharging resistance, and an equivalent parallel resistance (EPR) representing the self-discharging losses [23,24]. The EPR models leakage effects and affects only the long-term energy storage performance of the UC [25,26].

The amount of energy drawn from the UC bank is directly proportional to the capacitance and the change in the terminal voltage [8,25], given by

$$E_{\text{UC}} = \frac{1}{2}C(V_{\text{i}}^2 - V_{\text{f}}^2). \tag{11}$$

When the ultra-capacitor bank is subject to supply a prescribed amount of energy, the UC terminal voltage decreases. Eq. (11) represents the voltage variation versus energy released or captured by the ultra-capacitor bank. If the UC bank releases energy to the load side, E_{UC} is positive. If energy is captured by the UC bank, E_{UC} is negative.

The effective specific energy for a prescribed load can be supplied by various UC bank configurations. In practical applications, the required amount of terminal voltage and energy or the capacitance of UC storage system can be built using multiple UCs in series and parallel. The terminal voltage determines the number of capacitors which must be connected in series to form a bank and the total capacitance determines the number of capacitors which must be connected in parallel in the bank. The total resistance and the total capacitance of the UC bank may be calculated as [24,25]

$$R_{\text{UC-total}} = n_{\text{s}}\frac{\text{ESR}}{n_{\text{p}}}, \tag{12}$$

$$C_{\text{UC-total}} = n_{\text{p}}\frac{C}{n_{\text{s}}}. \tag{13}$$

The UC units can be arranged to build a UC bank, which is capable of providing the short-term peak load demand [24]. The UC bank model has been implemented in MATLAB and SimPowerSystems for this study.

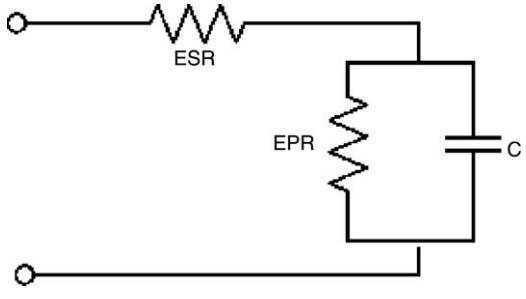

Fig. 4. Classical equivalent model for the UC unit.

2.5. Electrolyzer model

Water can be decomposed into its elementary components by passing electric current between two electrodes separated by an aqueous electrolyte [2,27,28]. The electrochemical reaction of water electrolysis is given by

$$\text{H}_2\text{O(l)} + \text{electrical energy} \Rightarrow \text{H}_2\text{(g)} + \frac{1}{2}\text{O}_2\text{(g)}. \tag{14}$$

The Electrolyzer model involves the following parameters:

F	Faraday constant [C kmol^{-1}]
i_{e}	electrolyzer current [A]
n_{c}	the number of electrolyzer cells in series
η_{F}	Faraday efficiency
n_{H_2}	produced hydrogen moles per second [mol s^{-1}]

According to Faraday's law, hydrogen production rate of an electrolyzer cell is directly proportional to the electrical current in the equivalent electrolyzer circuit [2].

$$n_{\text{H}_2} = \frac{\eta_{\text{F}} n_{\text{C}} i_{\text{e}}}{2F}. \tag{15}$$

The ratio between the actual and the theoretical maximum amount of hydrogen produced in the electrolyzer is known as Faraday efficiency. Assuming that the working temperature of the electrolyzer is 40 °C, Faraday efficiency is expressed by [2,27]

$$\eta_{\text{F}} = 96.5\text{e}^{(0.09/i_{\text{e}} - 75.5/i_{\text{e}}^2)} \tag{16}$$

According to the Eqs. (15) and (16), a simple electrolyzer model is developed using Simulink, which is illustrated in Fig. 5.

The input resistance of the electrolyzer is used to represent the voltage–current characteristics of the Von Hoerner electrolyzer [3,29] for two limit temperatures between 39 and 52 °C. In this model, the electrolyzer works on the operating point 45 A–50 V. Therefore, the dc bus of the electrolyzer is fixed at 400 V by using a two-level thyristor controlled bridge, and eight electrolyzer units are used in series (45 A–400 V) to produce the hydrogen.

2.6. Hydrogen storage system

The amount of hydrogen required by the PEMFC is sent directly from the electrolyzer system according to the relationship between the output power and the hydrogen requirement

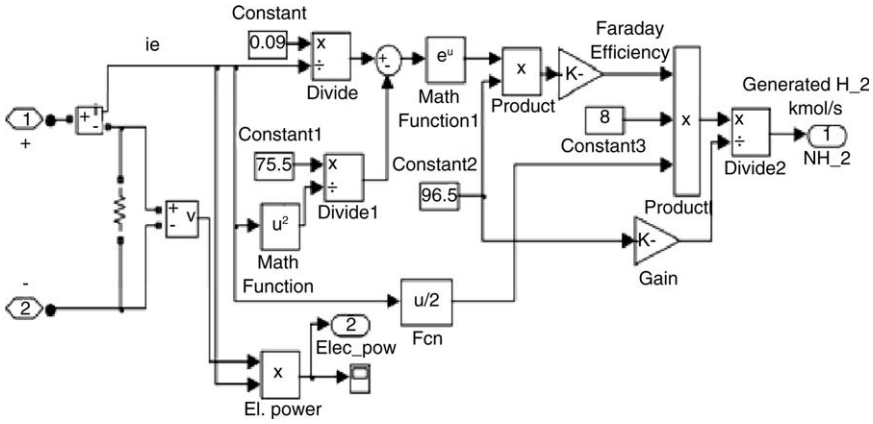

Fig. 5. The Simulink diagram of the electrolyzer model.

of the PEMFC system. The remaining amount of hydrogen (the difference between the produced and consumed hydrogen) is sent to the storage tank.

One of the hydrogen storage techniques is physical hydrogen storage, which involves using tanks to store either compressed hydrogen gas or liquid hydrogen. The hydrogen storage model is based on Eq. (17) and it directly calculates the tank pressure using the ratio of hydrogen flow to the tank. The produced hydrogen is stored in the tank, whose system dynamics can be expressed as follows [13]

$$P_b \hat{-} P_{bi} = z\frac{N_{H_2} R T_b}{M_{H_2} V_b}. \tag{17}$$

The parameters used in the hydrogen storage system are listed below:

M_{H_2}	molar mass of hydrogen [kg kmol^{-1}]
N_{H_2}	hydrogen moles per second delivered to the storage tank [kmol s^{-1}]
P_b	pressure of tank [Pa]
P_{bi}	initial pressure of the storage tank [Pa]
R	universal (Rydberg) gas constant [J (kmol °K)$^{-1}$]
T_b	operating temperature [°K]
V_b	volume of the tank [m^3]
z	compressibility factor as a function of pressure

Neither the compression dynamics nor the compression energy requirements are accounted for in our calculations. All auxiliary power requirements such as pumps, valves, fan and compression motors were ignored in the dynamic model. The Simulink version of the hydrogen storage model is depicted in Fig. 6.

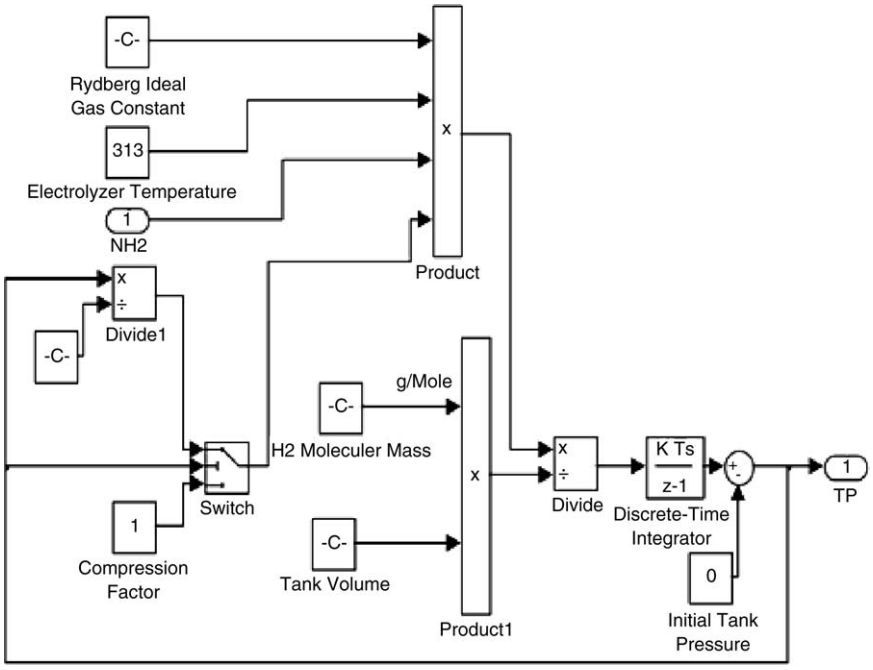

Fig. 6. The Simulink model of the hydrogen storage system.

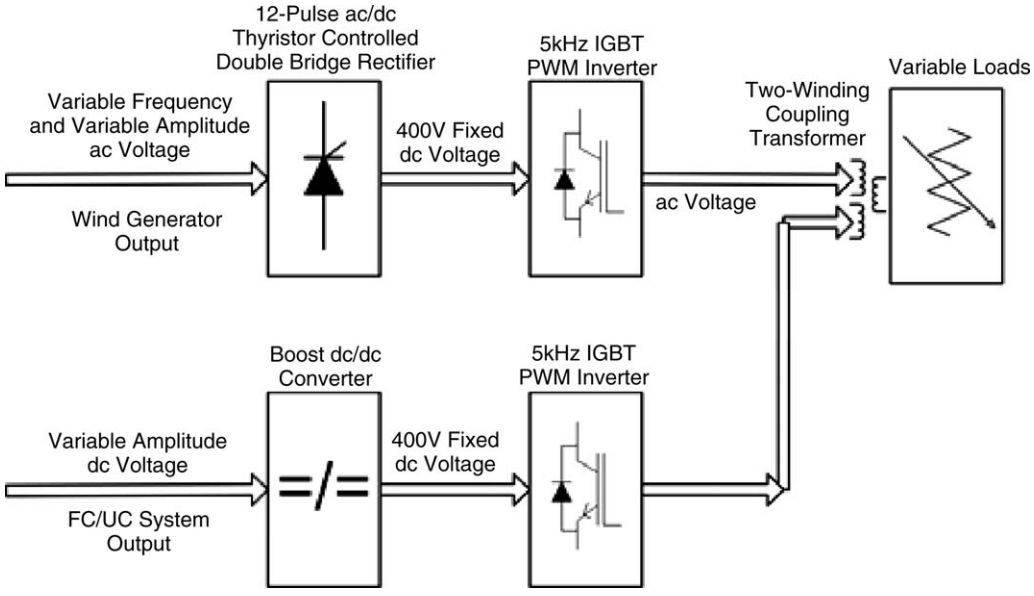

Fig. 7. The power controllers of the system buses.

2.7. Power conditioning units of the system buses

In the power control strategy used for the proposed technique, if the wind speed is sufficient to provide power to satisfy load demands and electrolyzer power requirements, then the wind turbine feeds the loads and the electrolyzer unit. The hydrogen produced by the electrolyzer is used in the FC system when wind power becomes lower than that required for the load demands. During normal operation, when the power demand exceeds the maximum power supplied by the FC, the excess power is supplied by the UC. To implement the aforementioned power management strategy, appropriate power control systems are used at relevant points and the total system components are integrated. In the proposed model, the power control systems are based on two fixed dc buses, and the power controllers used at the related system buses are depicted in Fig. 7.

2.7.1. Power conditioning of the wind turbine output

Due to the variations in wind speed, the output voltage of the generator coupled to the wind turbine experiences variations in frequency and amplitude. The generator voltage is rectified using a double-bridge converter instead of using a voltage and frequency regulator on the ac bus. The rectified voltage is fixed, which is then converted to ac voltage to overcome the fluctuations in the amplitude and frequency of the generator output voltage. In addition, this fixed dc bus is also used for the electrolyzer simultaneously. The schematic of the double-bridge rectifier is shown in Fig. 8.

An attractive feature of the double-bridge rectifier is that it causes less harmonic distortion effects on the source side thanks to the narrowed commutation periods. Another feature is the controllable dc output voltage with a 12-pulse synchronized PWM generator by tuning the firing angle α. The controllable ac/dc converter is used to smooth the wind turbine output power before being supplied to the electrolyzer. As reported in Ref. [3], fluctuations of the electrolyzer voltage may increase energy losses and generate impure hydrogen. Furthermore, efficient production and storage of hydrogen are major challenges that need further investigation [9]. Because the output of wind turbines varies with wind speed, and commercially available electrolyzers require a stable dc voltage [9].

To address the aforementioned factors, we used a thyristor controlled double-bridge rectifier to supply electrolyzer voltage using a novel topology. Since the dc bus voltage is controllable, the electrolyzer voltage can be controlled to track the reference voltage of 400 V. The firing angle α is controlled by a discrete PI controller. It is more efficient to use a fast controller for such a voltage tracker, when compared to using a mechanical blade degree control at the turbine tower. A mechanical blade controller is very slow and cannot tolerate the rapid changes of

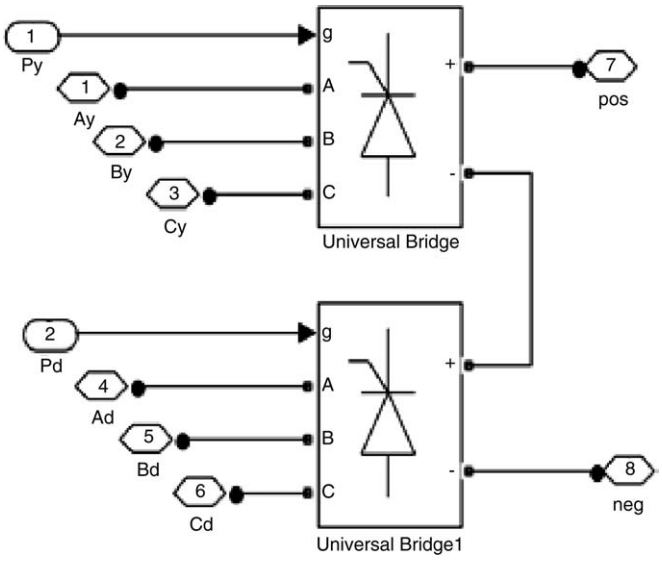

Fig. 8. The double-bridge thyristor controlled ac/dc converter.

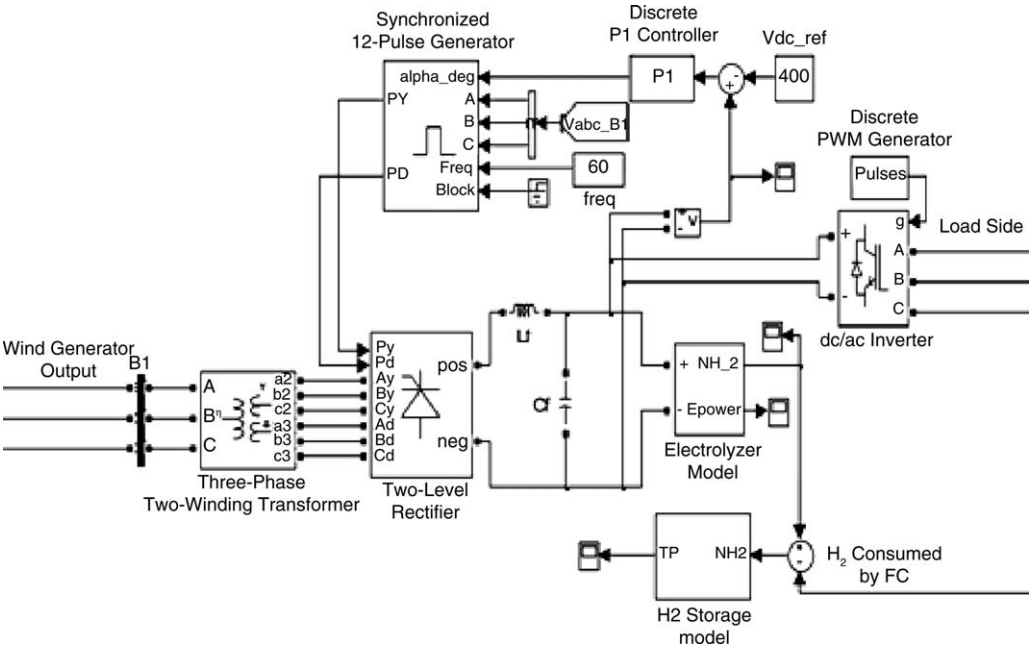

Fig. 9. The double-bridge rectifier, control system, filter elements, electrolyzer and hydrogen storage models.

wind speed because of the mechanical constraints like inertia and friction. The double-bridge rectifier requires a three-phase two-winding transformer to obtain six input ports with appropriate phase angles. The power conditioning units of the wind turbine output is depicted in Fig. 9.

2.7.2. UC bank charge–discharge control system

In this subsection, we present the charge/discharge control of the UC bank to perform load sharing with the FC system when they simultaneously operate with the wind turbine. Although FC systems exhibit good power supply capability during steady-state operation, the response of fuel cells during instantaneous and short-term peak power demand periods is relatively poor. In these periods, the UC bank can assist the FC system to achieve good performance [30] whereas reducing the cost and size of the FC system.

Various topologies may be used for integrating the UC with the FC power systems [24,25,30–32]. For example, the UC system integration can be done with or without power electronic converter via series and parallel connection. Because of the high specific power and power density of UC bank, it may be possible to eliminate the dc/dc converter for voltage regulation so that it can deliver higher output [24,30,31]. In this study, it is assumed that the UC bank may assist in power delivery only when the FC system is in operation. We integrated a UC bank with the FC system using two power diodes and two semiconductor power switches as shown in Fig. 10.

The power sharing between the FC system and UC bank is determined by the control switches (S1 and S2) according to the load demand. The main control algorithm for the FC and UC system can be summarized as follows:

- During low power demand (<32 kW), the FC system generates up to its load limit, and the excess power is used to charge the UC. In this case, FC system power is transported to dc bus over the D1 diode and the UC is charged over the D1 diode and closing the S1 switch. The UC does not provide any power since the S2 switch is open.
- During high power demand (≥32 kW) periods, the FC system generates the rated power. Also, the UC is discharged to meet the extra power requirements that cannot be supplied by the FC system. In this case, FC system power is transported to the dc bus over the D1 diode, and the UC is discharged over the S2 switch and D2 diode to satisfy the excess load demand. In this situation, no reverse current can flow to the FC system from the UC bank due to the blocking D1 diode. Also, the UC bank cannot draw power from FC system during discharging to avoid overloading the FC system, which is achieved by keeping S1 switch open.

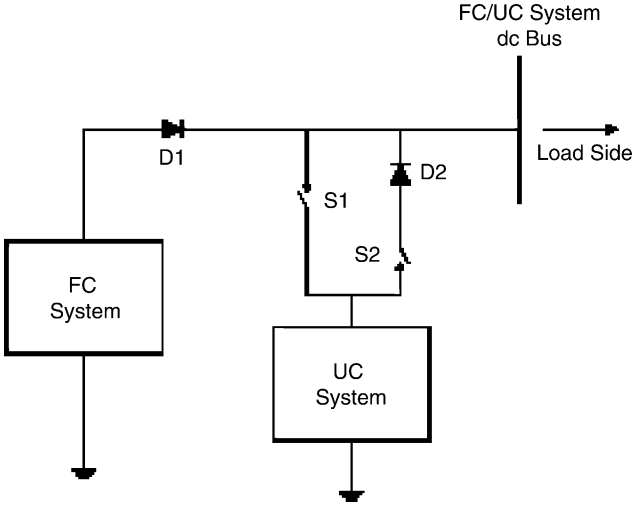

Fig. 10. The FC/UC hybrid system.

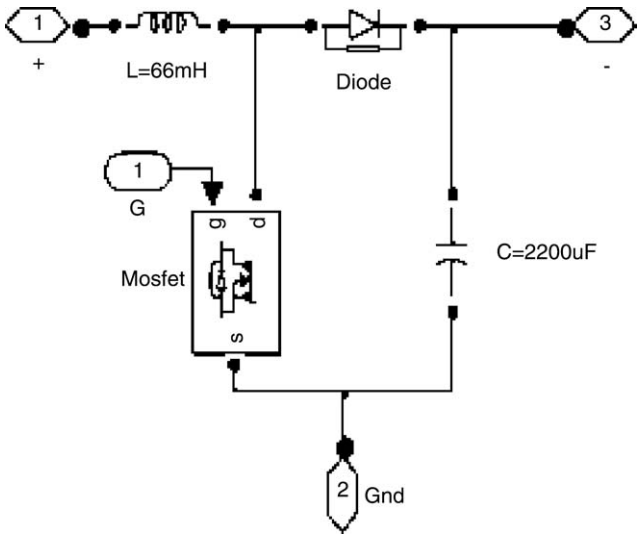

Fig. 11. Boost type dc/dc converter for the FC/UC dc bus.

To realize the control system for the aforementioned FC and UC models, control algorithm, ideal switching elements, and current and voltage sensors are used in the simulation model.

2.7.3. FC/UC system output power control

The increase in load power decreases the FC output voltage according to the model dynamics. Therefore, a boost type dc/dc converter is used at the FC/UC system bus to maintain 400 V output voltage. The topology of the boost type dc/dc converter is given in Fig. 11.

In the converter, the gate signal of the MOSFET is obtained using a discrete PI controller-based system which determines the duty cycle according to the load side voltage. The PI controlled voltage tracking system is shown in Fig. 12.

2.7.4. dc/ac inverters for load side

The above mentioned two fixed dc voltages are converted to ac voltages with IGBT PWM inverters as shown in Fig. 7. Since these inverters have the same fixed dc inputs, both are controlled to produce three-phase ac output voltage with the same specifications (such as amplitude and frequency) using an appropriate PWM generator, which provides gate signals for the

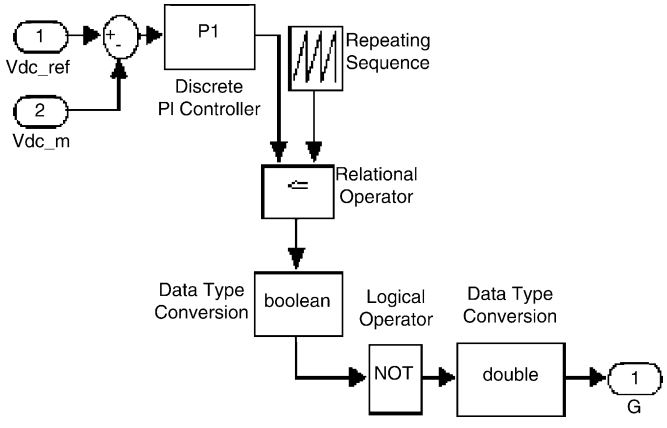

Fig. 12. dc/dc converter controller.

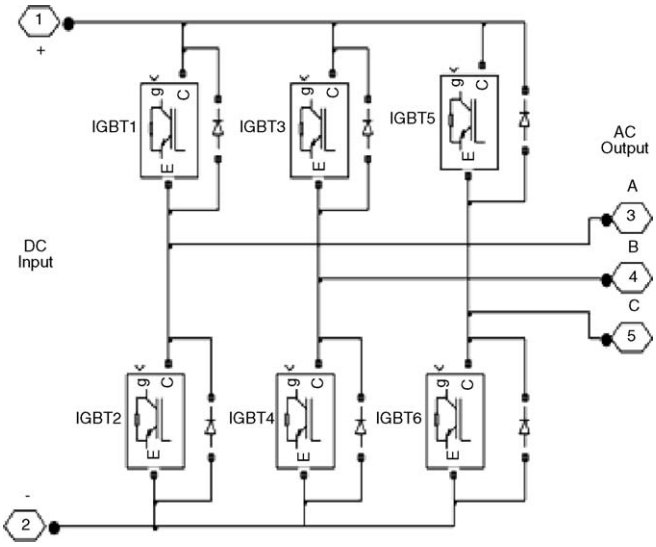

Fig. 13. dc/ac inverter model.

inverter elements. The three-phase IGBT inverter is shown in Fig. 13.

The parameters used in the voltage equations of the inverter are as follows:

m	modulation index
V_{dc}	dc input voltage of the inverter [V]
$V_{l\text{-}l}$	Line-to-line output voltage of the inverter [V]

In PWM inverters, the amplitude of the output ac voltage is a function of the dc input voltage and modulation index. The line-to-line output voltage of such an inverter can be expressed as

$$V_{l\text{-}l} = \frac{\sqrt{3}}{2\sqrt{2}} m V_{dc}. \tag{18}$$

3. Simulation results and discussion

The block diagram of the integrated wind/FC/UC system and the power controllers are shown in Figs. 1 and 7, respectively. At first, the wind turbine, induction generator, FC system, UC bank and the power controller system are described in this section. For the wind turbine dynamics, a generic equation is used to model c_p (λ, β), which is based on the turbine model characteristics of Ref. [19], given by

$$c_p(\lambda,\ \beta) = c_1 \left(\frac{c_2}{\lambda_i} - c_3\beta - c_4 \right) e^{(c_5/\lambda_i)} + c_6\lambda \tag{19}$$

where

$$\frac{1}{\lambda_i} = \frac{1}{\lambda + 0.08\beta} - \frac{0.035}{\beta^3 + 1}. \tag{20}$$

The coefficients values used are: $c_1 = 0.5176$, $c_2 = 116$, $c_3 = 0.4$, $c_4 = 5$, $c_5 = 21$ and $c_6 = 0.0068$. The maximum value of c_p, ($c_p = 0.48$) is achieved for $\beta = 0^\circ$ and $\lambda = 8.1$. This par-

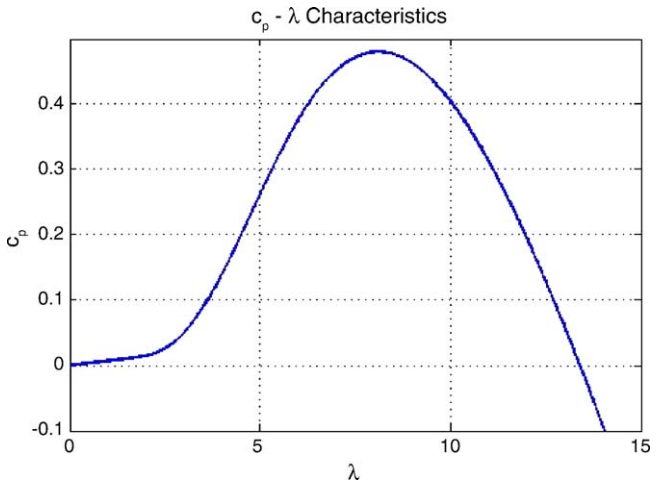

Fig. 14. c_p–λ characteristics of the wind turbine.

ticular value of λ is defined as the nominal value. The λ–c_p characteristic of the turbine is illustrated in Fig. 14 for $\beta = 0°$.

The generator speed (rpm) and the generator power (p.u.) characteristics are shown in Fig. 15 corresponding to various wind speed values.

The parameters of the induction generator are given in Table 1. The base values are the rated power and the voltage values of the generator for the parameters given in per unit (p.u.).

The PEMFC system operates with the UC bank connected in parallel using the configuration given in Fig. 10. The voltage drops on the D1 and D2 diodes are assumed to be 0.8 V, and the internal resistance of switches S1 and S2 are assumed be 0.001 Ω. For the simulated model, the parameters of the Maxwell Boostcap® PC2500 UC unit are used and the characteristics of UC unit are shown in Table 2.

Each UC unit has a nominal voltage of 2.5 V corresponding to 2700 F. Assuming a 400 V dc output from the FC system, a string of 160 UCs in series (16.875 F per string) is used to represent 400 V and the initial voltage of the UC bank is set to be 363.5 V. The energy is stored in a 16.875 F capacitance at 400 V. This size of the UC can be changed to suit various power capacities for different applications.

The PEMFC system parameters are given in Table 3 [22] and the initial active output power of the FC system is assumed to be 2 kW.

The parameters of the double-bridge rectifier are given in Table 4.

The parameters of the boost type dc/dc converter located at the output of the FC/UC system are given in Table 5.

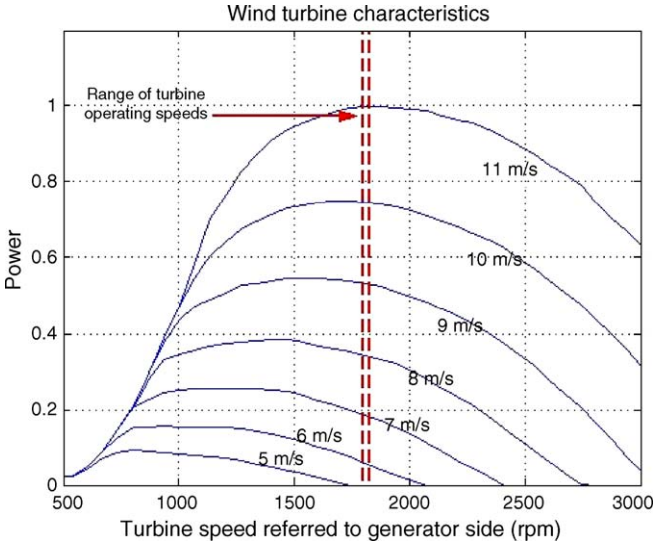

Fig. 15. Wind turbine characteristics.

Table 1
Induction generator parameters

Nominal power ($P_{mechanic}$)	200 [HP]
Nominal voltage (line-to-line)	460 [V]
Nominal frequency	60 [Hz]
Nominal revolutions per minute	1785 [rpm]
Rotor type	Squirrel cage
Stator resistance	0.01282 [p.u.]
Stator inductance	0.05051 [p.u.]
Rotor resistance	0.00702 [p.u.]
Rotor inductance	0.05051 [p.u.]
Inertia constant	0.3096 [s]
Friction factor	0.0114 [p.u.]
Pairs of poles	2

Table 2
Maxwell Boostcap® PC2500 UC characteristics [33]

UC Parameters	Value
Capacitance	2700 ± 20% [F]
Internal resistance (dc)	0.001 ± 25% [Ω]
Leakage current	0.006 [A], 72 h, 25 °C
Operating temperature	−40 °C to 65 °C
Rated current	100 [A]
Voltage	2.5 [V]
Volume	0.6 [l]
Weight	0.725 [kg]

Table 3
FC system model parameters

Activation voltage constant (B)	0.04777 [A^{-1}]
Activation voltage constant (C)	0.0136 [V]
Conversion factor (CV)	2
Faraday's constant (F)	96484600 [C $kmol^{-1}$]
Hydrogen time constant (τ_{H_2})	3.37 [s]
Hydrogen valve constant (K_{H_2})	4.22×10^{-5} [kmol (s atm)$^{-1}$]
Hydrogen–oxygen flow ratio (r_{H-O})	1.168
K_r constant = $N_0/4F$	1.8449×10^{-6} [kmol (s A)$^{-1}$]
Methane reference signal ($Q_{methref}$)	0.000015 [k mol s^{-1}]
No load voltage (E_0)	0.6 [V]
Number of cells (N_0)	712
Oxygen time constant (τ_{O_2})	6.74 [s]
Oxygen valve constant, (k_{O_2})	2.11×10^{-5} [kmol (s atm)$^{-1}$]
FC internal resistance (R_{int})	0.00303 [Ω]
FC absolute temperature (T)	343 [K]
Universal gas constant (R)	8314.47 [J (kmol K)$^{-1}$]
Utilization factor (U)	0.8
Water time constant (τ_{H_2O})	18.418 [s]
Water valve constant (K_{H_2O})	7.716×10^{-6} [kmol (s atm)$^{-1}$]

Table 4
Double-bridge rectifier model parameters

Snubber resistance of one thyristor	2 [kΩ]
Snubber capacitance of one thyristor	0.1 [μF]
Internal resistance of one thyristor	1 [mΩ]
Pulse width of synchronized 12-pulse generator	80 [°]
Filter inductance	66 [mH]
Filter capacitance	3300 [μF]
Proportional gain of PI voltage control system	2
Integral gain of PI voltage control system	20
Reference voltage	400 [V]

Table 5
dc/dc converter model parameters

Converter inductance	66 [mH]
Converter capacitance	2200 [μF]
Semiconductor type	MOSFET
Rated switching frequency	1000 [Hz]
Proportional gain of PI voltage control system	0.0001
Integral gain of PI voltage control system	0.01
Reference voltage	400 [V]

Table 6
dc/ac inverter model parameters

Semiconductor type	IGBT-DIODE
Snubber resistance	2 [kΩ]
Snubber capacitance	0.1 [μF]
Internal resistance	1 [mΩ]
Carrier frequency	5 [kHz]
Modulation index	0.98
Frequency of output voltage	60 [Hz]

The dc/ac inverters have the parameter values as shown in Table 6.

These inverters are both controlled to produce three-phase ac output voltage with a frequency of 60 Hz, and modulation index of 0.98. Thus, the line-to-line voltage of the inverter output is 240 V, which is calculated using Eq. (18). Finally, Table 7 shows the parameters of the input transformer used in the two bridge rectifier.

In this work, the load demand of the user is satisfied using the wind/FC/UC hybrid topology described earlier. If the power demand is greater than the power available from the wind turbine, the FC system satisfies the excess power needed. The UC bank serves as a short duration power source to meet the excess power that cannot be satisfied by the FC system. A wind turbine,

Table 7
Transformer parameters

Nominal power	120 [kW]
Nominal frequency	60 [Hz]
Input winding parameters (Yg) [V1 R1 L1]	460 [V], 0.00025 [p.u.], 0 [p.u.]
Output winding parameters (*Y*) [V2 R2 L2]	230 [V], 0.00025 [p.u.], 0.0024 [p.u.]
Output winding parameters (Delta) [V3 R3 L3]	230 [V], 0.00025 [p.u.], 0.0024 [p.u.]
Magnetization resistance	650 [Ω]
Magnetization reactance	650 [Ω]

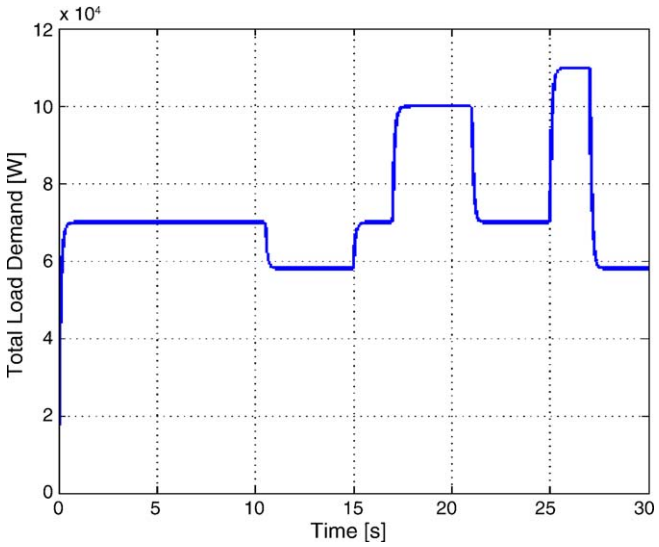

Fig. 16. Total load demand of the user.

a FC system and a UC bank are used in above mentioned hybrid topology to meet the user load profile as shown in Fig. 16.

To observe the dynamic behavior of the system, the wind profile shown in Fig. 17 is used. The dynamic model used for simulations is highly nonlinear and has a stiff structure, and it takes over half an hour to complete the simulation with a 1.6 GHz microprocessor-based computer (1 GB RAM). Consequently, a 30-s duration is used for the simulations with a fall in wind speed at about the 10th second in wind speed profile. This sudden fall in wind speed affects the power produced by the induction generator coupled to the wind turbine as well as the electrolyzer voltage as observed in Figs. 18 and 19, respectively.

From Figs. 18 and 19, we observe that although the available power from the wind generator decreases because of the wind speed, the PI controlled firing angle of the double-bridge rectifier maintains the electrolyzer voltage at 400 V. If the PI controller is not used to control the firing angle of the rectifier and in the

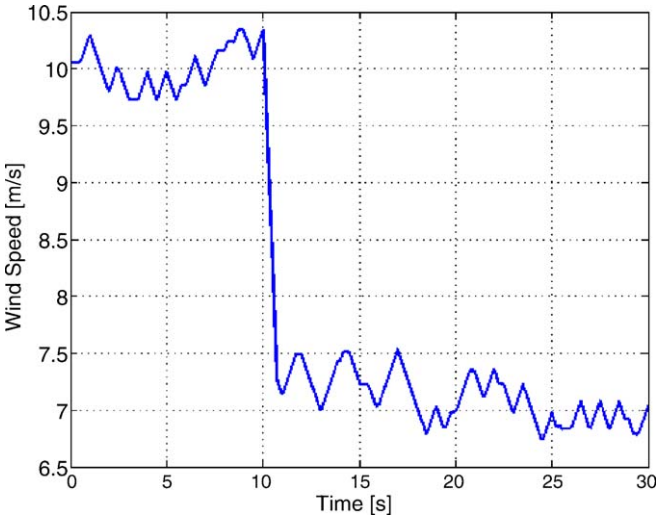

Fig. 17. Wind profile used for system simulation.

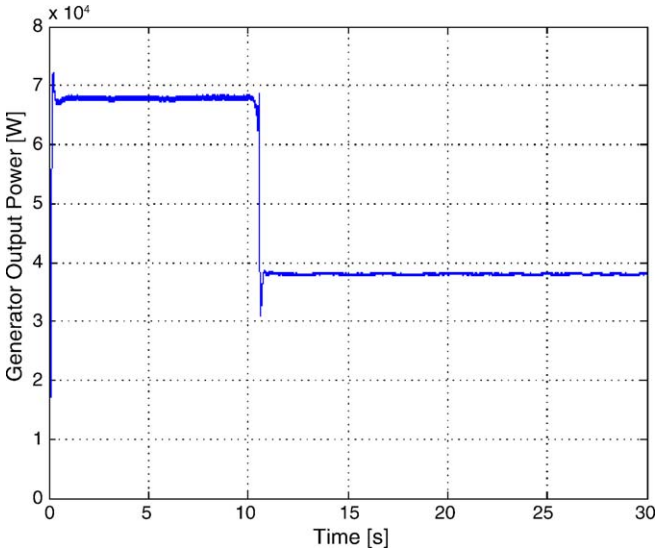

Fig. 18. Power of the generator coupled to the wind turbine.

absence of the load management strategy, the dc bus voltage and the wind power would collapse as illustrated in Figs. 20 and 21, respectively.

The amount of hydrogen moles produced per second corresponding to the electrolyzer voltage given in Fig. 19, is shown in Fig. 22.

The wind turbine output including power delivered to the load side and power delivered to the electrolyzer is shown in Fig. 18. Although the turbine output power decreases, the nominal power of 18 kW can be supplied to the electrolyzer. Since wind turbine output power does not decrease below 18 kW in the simulation, the hydrogen production rate of the electrolyzer stays the same as shown in Fig. 22.

In this study, the minimum power drawn from the FC system is set to be of 2 kW in order to keep the FC system ready to provide larger amounts of power. After the wind power decreases, the difference between the load demand and the wind power is

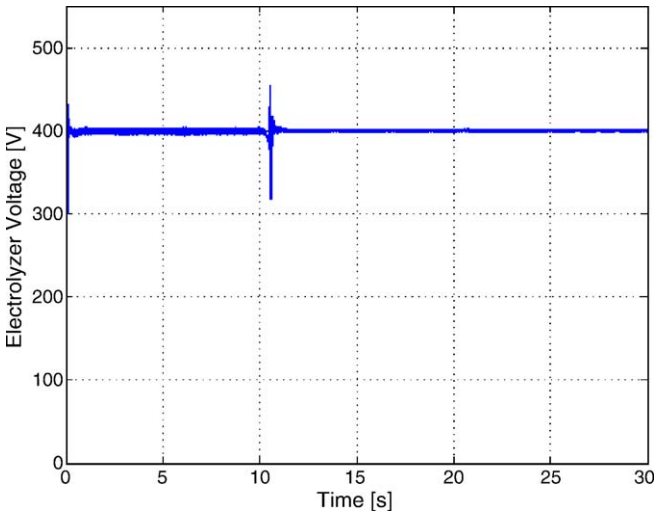

Fig. 19. Electrolyzer voltage (dc bus voltage of wind turbine output).

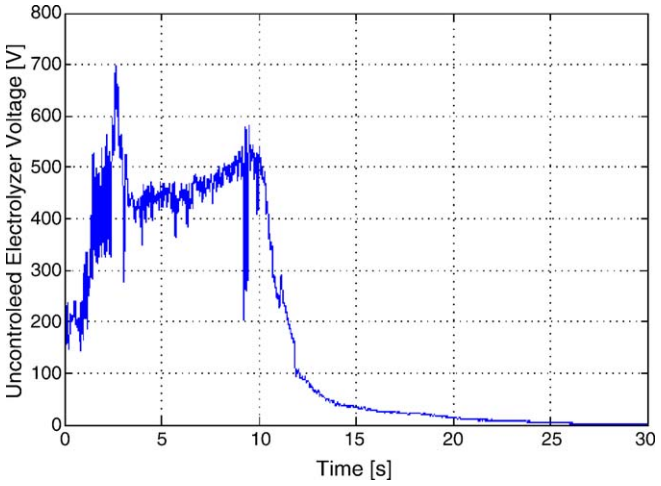

Fig. 20. Electrolyzer voltage without PI controller.

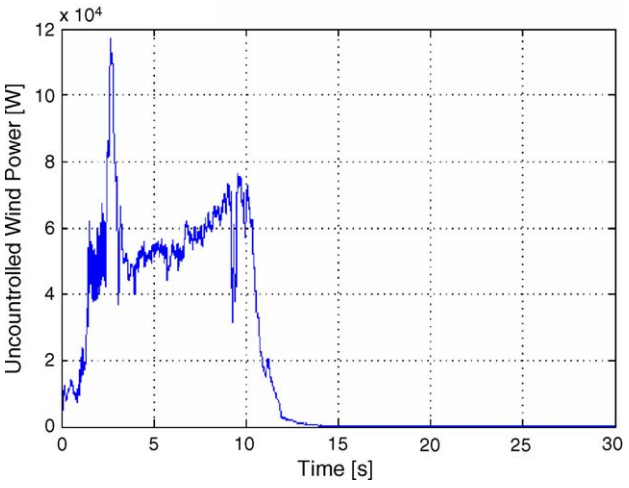

Fig. 21. Wind power without PI controller.

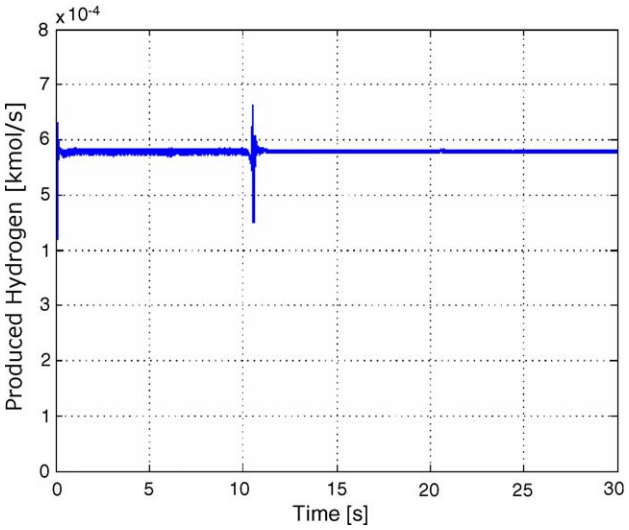

Fig. 22. Produced amount of hydrogen.

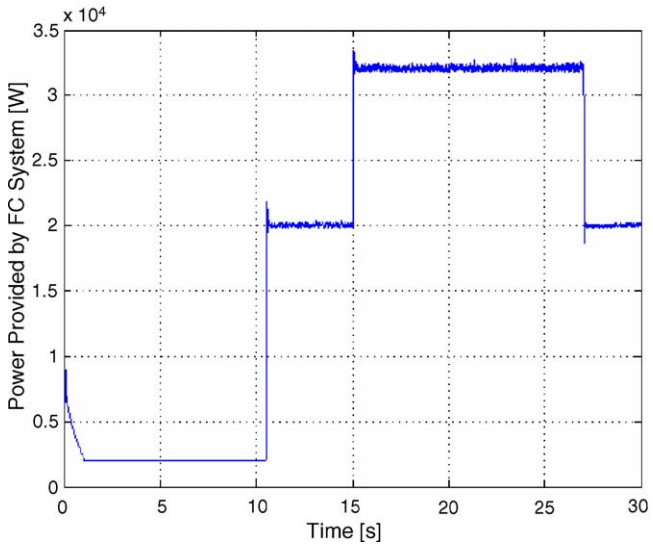

Fig. 23. Load power satisfied by FC system.

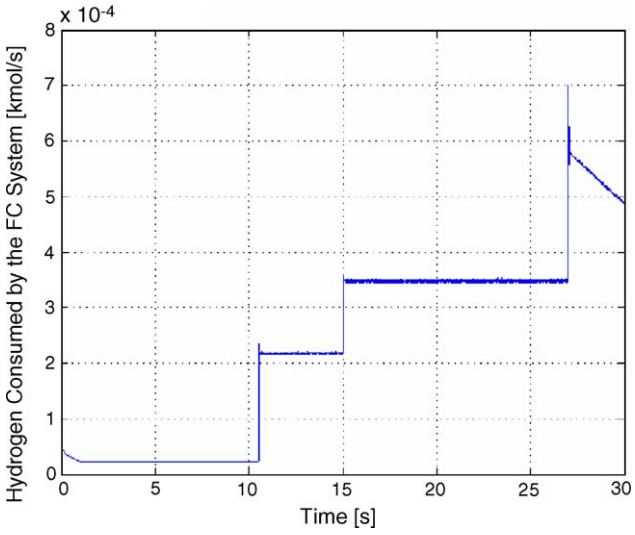

Fig. 25. Hydrogen moles per second consumed by FC system.

satisfied by FC system. The load power satisfied by FC system measured from ac side is depicted in Fig. 23.

Corresponding to the load profile shown in Fig. 16, we observe that the increment of load demand after the 15th second is met by FC system, and the FC power increases up to its maximum value as shown in Fig. 23. It may be mentioned that the power satisfied by FC system depicted in Fig. 23 inherently changes the internal voltage of the FC system as shown in Fig. 24. The internal voltage of FC system decreases when the FC output power increases. This relation between power and the voltage of the FC system authenticates the reliability of the FC model.

The transient response of the FC system voltage to the load changes varies according to the amount of power supplied by the FC system as shown in Fig. 24.

The amount of hydrogen moles consumed by the FC system is proportional to the power drawn from the FC system. The hydrogen flow to the FC system per second is depicted in Fig. 25.

The hydrogen flow to the storage tank is shown in Fig. 26. The amount of hydrogen to be stored in the storage tank corresponds to the difference between the hydrogen produced by the electrolyzer and the hydrogen consumed by the FC system.

The hydrogen storage tank pressure variation corresponding to the amount of hydrogen delivered to the storage tank is shown in Fig. 27. From Fig. 27, it is evident that the hydrogen storage tank pressure increases with time as more and more hydrogen moles delivered to the tank. Fig. 27 also demonstrates that the slope of the pressure is proportional to the amount of hydrogen delivered to the storage tank.

According to the power profile depicted in Fig. 16, peak load demands would be observed between 17 and 21 s and from 25 to 27 s. During these time intervals, the FC power is at its maximum value and also no increment is observed for the wind speed. In this situation, UC discharges to the dc bus. The peak load demand is satisfied by UC bank and measured from ac side as shown in Fig. 28.

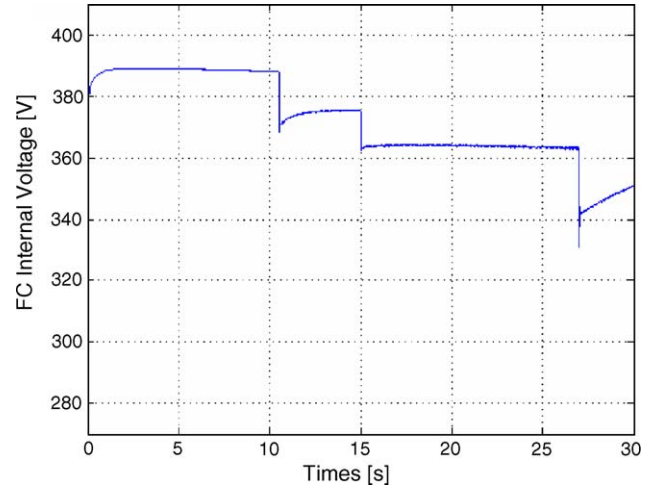

Fig. 24. Internal voltage of the FC system.

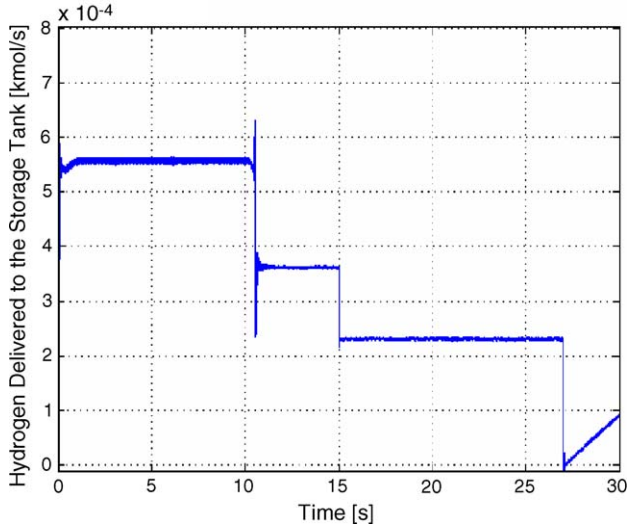

Fig. 26. Hydrogen moles per second delivered for storage in the tank.

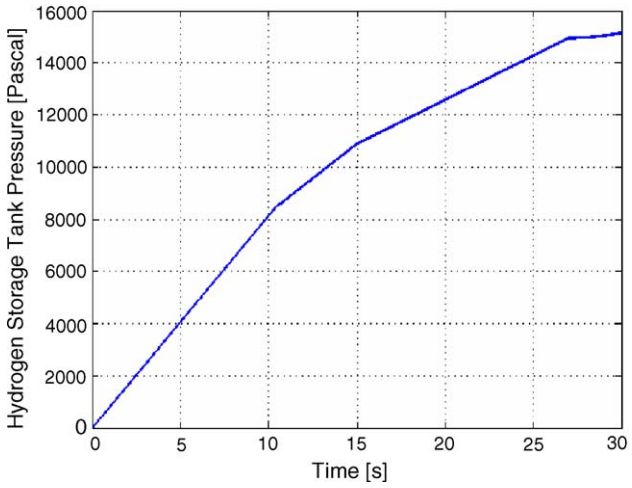

Fig. 27. Hydrogen storage tank pressure.

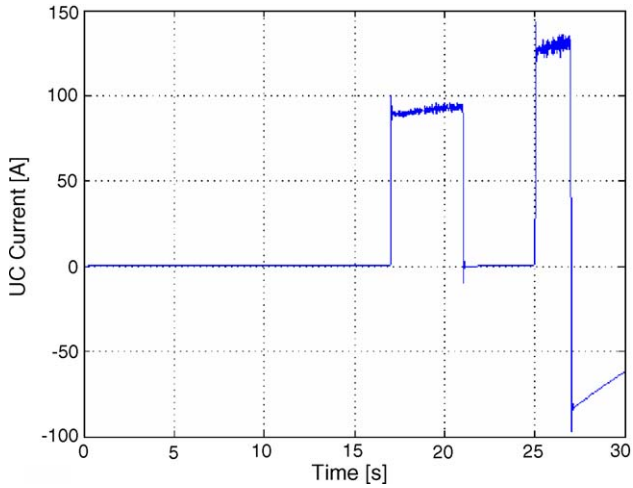

Fig. 29. UC current change with respect to power demand.

The power met by the UC introduces a current change at the UC bank terminals as depicted in Fig. 29.

According to Fig. 29, the UC current before the 17th second is of zero. When the UC current is positive (time intervals 17–21 and 25–27), energy is transferred to the dc bus by the UC bank. When the UC current is negative (time intervals 27–30), the UC bank is recharged. The UC bank cannot be recharged after the first discharging period because during this period the FC operates at the maximum power output. The UC bank is recharged only after the 27th second when the load demand decreases and the remaining power is provided to the UC bank for recharging. Fig. 30 shows the UC bank voltage variation during charge and discharge states. It is obvious from Fig. 30 that the UC bank voltage decreases while the energy transfer to the load side increases during recharging.

At the beginning of the simulation, the initial voltage of the UC bank is 363.5 V. A voltage decrease occurs in the UC bank terminal voltage when supplying a prescribed amount of energy. For instance, in the time interval from 17 to 21 s, the UC bank is required to supply 30000 W × 4 s = 120,000 W s, and the voltage drops from 363.5 to 343.38 V. When the fuel cell output power is not exceeded, the UC recovers the released energy until the UC terminal voltage reaches the FC system output voltage (refer to Eq. (11)).

Although the UC and FC system voltages fluctuate due to load variations, the dc/dc converter of the FC/UC system successfully keeps the load voltage stable. The output voltage of the dc/dc converter is depicted in Fig. 31 where the high voltage in the first few moments corresponds to transients and damps out very fast.

The PI controlled double-bridge ac/dc converter at the output of the wind turbine and the PI controlled dc/dc converter at the output of the FC/UC system keep these dc buses fixed at 400 V as shown in Figs. 19 and 31, respectively. Since the voltage of the two dc buses is kept at 400 V, dc/ac inverters are used to deliver the required power to the load side at 60 Hz frequency and 240 V line-to-line voltage.

The power delivered to the load side by the wind/FC/UC hybrid topology is illustrated in Fig. 32.

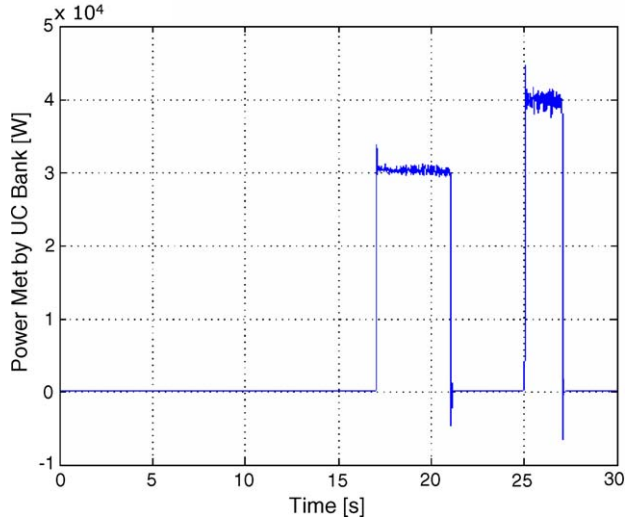

Fig. 28. Power satisfied by UC bank.

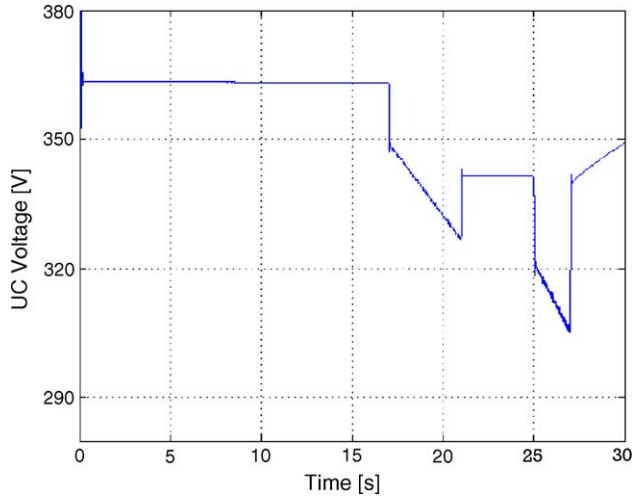

Fig. 30. UC bank voltage variation as a function of time.

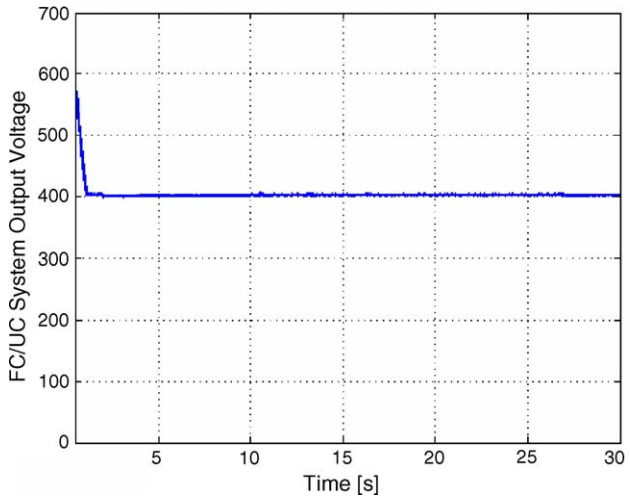

Fig. 31. Output voltage of the dc/dc converter.

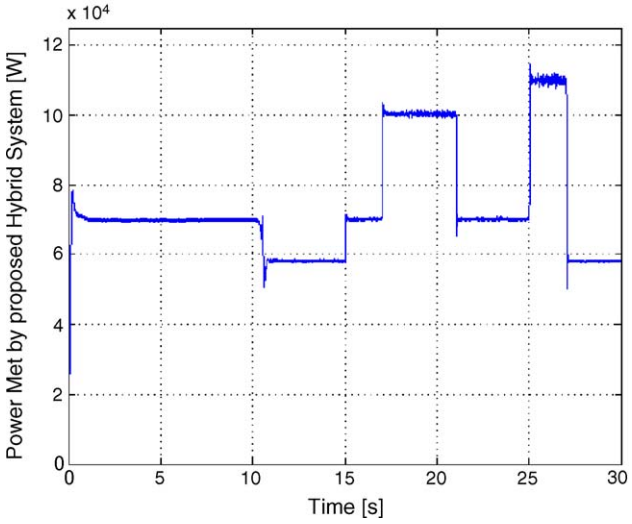

Fig. 32. Power delivered to load side by the hybrid topology.

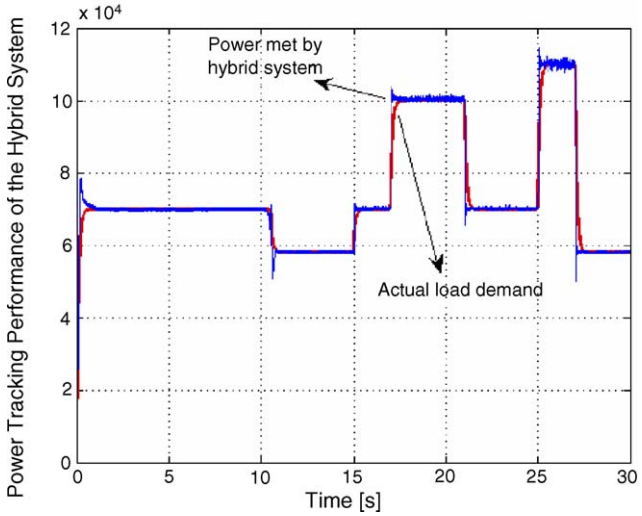

Fig. 33. Power tracking performance of the hybrid topology.

Finally, the user power requirement and the power delivered to the load side by the wind/FC/UC hybrid system are illustrated in Fig. 33. In Fig. 16, the total load demand is shown, which should be supplied by the wind/FC/UC system. Due to the physical constraints such as time constants, control delays and measurement errors, there is a little difference between the load demand and the power supplied as shown in Fig. 33. Under these constraints, the system can successfully accommodate wind speed changes and the control system can efficiently track the load demand.

4. Conclusions

In this paper, a novel wind/FC/UC hybrid power system is designed and modeled for a grid-independent user with appropriate power flow controllers. The available power from the renewable energy sources is highly dependent on environmental conditions such as wind speed. To overcome this deficiency of the wind system, we integrated wind turbine with the FC/UC system using a novel topology. This hybrid topology exhibits excellent performance under variable wind speed and load power requirements. The proposed system can be used for non-interconnected remote areas or isolated cogeneration power systems with non-ideal wind speed characteristics.

Acknowledgement

This work was supported in part by the U.S. Department of Energy under Grant DE-FG02-02ER63376.

References

[1] The Energy Foundation Annual Report, The Energy Foundation, San Francisco, CA, 2001.
[2] M.J. Khan, M.T. Iqbal, Dynamic modeling and simulation of a small wind-fuel cell hybrid energy system, J. Renewable Energy 30 (3) (2005) 421–439.
[3] H. De Battista, R.J. Mantz, F. Garelli, Power conditioning for a wind-hydrogen energy system, J. Power Sources 155 (2) (2006) 478–486.
[4] U.S. Department of Energy, Energy Efficiency and Renewable Energy, Wind & Hydropower Technologies Program, Wind Energy Research Area, http://www.eere.energy.gov.
[5] M.C. Williams, J.P. Strakey, S.C. Singhal, U.S. distributed generation fuel cell program, J. Power Sources 131 (1–2) (2004) 79–85.
[6] R.M. Dell, D.A.J. Rand, Energy storage—a key technology for global energy sustainability, J. Power Sources 100 (1–2) (2001) 2–17.
[7] B.D. Shakyaa, Lu Ayea, P. Musgraveb, Technical feasibility and financial analysis of hybrid wind-photovoltaic system with hydrogen storage for Cooma, Int. J. Hydrogen Energy 30 (1) (2005) 9–20.
[8] A. Burke, Ultracapacitors: why, how and where is the technology, J. Power Sources 91 (1) (2000) 37–50.
[9] F.I. Khan, K. Hawboldt, M.T. Iqbal, Life cycle analysis of wind-fuel cell integrated system, J. Renewable Energy 30 (2) (2005) 157–177.
[10] B. Delfino, F. Fornari, Modeling and control of an integrated fuel cell-wind turbine system, in: Proceedings of the IEEE PowerTech Conference, Bologna, vol. 2, 2003, p. 6.
[11] D.A. Bechrakis, E.J. McKeogh, P.D. Gallagher, Simulation and operational assessment for a small autonomous wind-hydrogen energy system, J. Energy Conversion Manage. 47 (1) (2006) 46–59.
[12] F. Barbir, PEM electrolysis for production of hydrogen from renewable energy sources, J. Solar Energy 78 (5) (2005) 661–669.
[13] H. Gorgun, Dynamic modeling of a proton exchange membrane (PEM) electrolyzer, Int. J. Hydrogen Energy 31 (1) (2006) 29–38.

[14] M. Uzunoglu, M.S. Alam, Dynamic modeling, design and simulation of a combined PEM fuel cell and ultra-capacitor system for stand alone applications, IEEE Trans. Energy Conversion, accepted for publication.
[15] M. Uzunoglu, A. Kizil, O.C. Onar, Her Yonu ile MATLAB (Proficiency in MATLAB, second ed.), Turkmen Kitabevi, Istanbul, 2003.
[16] MATLAB Simulink Simulation and Model Based Design User's Guide, Version 6.3, http://www.mathworks.com/access/helpdesk/help/pdf doc/simulink/sl using.pdf.
[17] MATLAB SimPowerSystems for Use with Simulink User's Guide, Version 4.1.1, http://www.mathworks.com/access/helpdesk/help/pdf doc/physmod/powersys/powersys.pdf.
[18] E.S. Abdin, W. Xu, Control design and dynamic performance analysis of a wind turbine-induction generator unit, IEEE Trans. Energy Conversion 15 (1) (2000) 91–96.
[19] S. Heier, Grid Integration of Wind Energy Conversion Systems, John Wiley & Sons Ltd, New York, 1998.
[20] E. Muljadi, C.P. Butterfield, Pitch-controlled variable-speed wind turbine generation, IEEE Trans. Industry Appl. 37 (1) (2001) 240–246.
[21] P.C. Krause, O. Wasynczuk, S.D. Sudhoff, Analysis of Electric Machinery, Wiley-IEEE Press, 2002.
[22] M.Y. El-Shark, A. Rahman, M.S. Alam, P.C. Byrne, A.A. Sakla, T. Thomas, A dynamic model for a stand-alone PEM fuel cell power plant for residential applications, J. Power Sources 138 (1–2) (2004) 199–204.
[23] R.M. Nelms, D.R. Cahela, B.J. Tatarchuk, Modeling double-layer capacitor behavior using ladder circuits, IEEE Trans. Aerospace Electron. Syst. 39 (2) (2003) 430–438.
[24] K.H. Hauer, Analysis tool for fuel cell vehicle hardware and software (controls) with an application to fuel cell economy comparisons of alternative system designs, Ph.D. Dissertation, Department of Transportation Technology and Policy, University of California Davis, 2001.
[25] R.L. Spyker, R.M. Nelms, Analysis of double-layer capacitors supplying constant power loads, IEEE Trans. Aerospace Electron. Syst. 36 (4) (2000) 1439–1443.
[26] R.L. Spyker, R.M. Nelms, Classical equivalent circuit parameters for a double-layer capacitor, IEEE Trans. Aerospace Electron. Syst. 36 (3) (2000) 829–836.
[27] O. Ulleberg, Stand-alone power systems for the future: optimal design. Operation and Control of Solar-Hydrogen Energy Systems, PhD Dissertation, Norwegian University of Science and Technology, 1998.
[28] K. Sapru, N.T. Stetson, S.R. Ovshinsky, Development of a small scale hydrogen production storage system for hydrogen applications, in: Proceedings of the 32nd Intersociety Conference, vol. 3, 1997, pp. 1947–1952.
[29] T. Schucan, Case studies of integrated hydrogen energy systems, International Energy Agency Hydrogen Implementing Agreement, Final Report, Paul Scherrer Institute, Switzerland, 2000.
[30] Honda fuel cell power FCX (2004). http://world.honda.com/FuelCell/FCX/FCXPK.pdf.
[31] L. Gao, R.A. Dougal, S. Liu, Power enhancement of an actively controlled battery/ultracapacitor hybrid, IEEE Trans. Power Electron. 20 (1) (2005) 236–243.
[32] M. Cacciato, F. Caricchi, F. Giuhlii, E. Santini, A critical evaluation and design of bi-directional dc/dc converters for super-capacitors interfacing in fuel cell applications, in: Proceedings of the 39th IAS Annual Meeting IEEE Industry Appl. Conference, vol. 2, 2004, pp. 1127–1133.
[33] Electric Double Layer Capacitor: BOOSTCAP® Ultracapacitor http://www.maxwell.com/pdf/uc/datasheets/PC2500.pdf\.

O.C. Onar received the BSc degree in electrical engineering from Yildiz Technical University, Turkey, in 2004. He is a research assistant at Yildiz Technical University and a research scholar in Electrical and Computer Engineering Department at the University of South Alabama. His research interests include alternative energy sources, fuel cells, energy conversion, power system modeling, analysis and control, power quality, active harmonic and EMI filtering in nonlinear systems and power system stability.

M. Uzunoglu received the BSc, MSc, and PhD degrees in electrical engineering from Yildiz Technical University, Turkey, in 1991, 1996 and 2000, respectively. He is a faculty member at Yildiz Technical University and a research scholar in the Electrical and Computer Engineering Department at the University of South Alabama. His research interests include alternative energy sources, fuel cells, energy conversion, power system modeling, analysis and control, power quality, voltage stability, artificial neural network, wavelet transformations, and state estimation.

M.S. Alam is a Professor and Chair of the ECE Department at the University of South Alabama (USA). His research interests include ultrafast computer architectures and algorithms, image processing, pattern recognition, fiber-optics, infrared systems, digital system design, and smart energy management and control. He is the author or co-author of more than 325 published papers, including 136 articles in refereed journals, 185 papers in conference proceedings, and 12 book chapters. He received numerous excellences in research, teaching and service awards including the 2005 Outstanding Scholar of the Year award from the USA Alumni Association. He served or serves as the PI or Co-PI of many research projects totaling nearly 13 M dollars, supported by NSF, FAA, DoE, ARO, AFOSR, WPAFB, SMDC, and ITT industry. Dr. Alam presented over 60 invited papers, seminars and tutorials at international conferences and research institutions in USA and abroad. He is a Fellow of OSA, a Fellow of the SPIE, a Fellow of IEE (UK), a senior member of IEEE, a member of ASEE and AIP. He was the Chairman of the Fort Wayne Section of IEEE for 1995–1996.